Stepwise Conformational Transitions of Stimuli-Responsive Linear Ternary Heterografted Bottlebrush Polymers in Aqueous Solution

*Michael T. Kelly, Ethan W. Kent, and Bin Zhao**

Department of Chemistry, University of Tennessee, Knoxville, Tennessee 37996, United States

* Corresponding author. Email: bzhao@utk.edu (B.Z.)

TOC Graphic

For Table of Contents use only

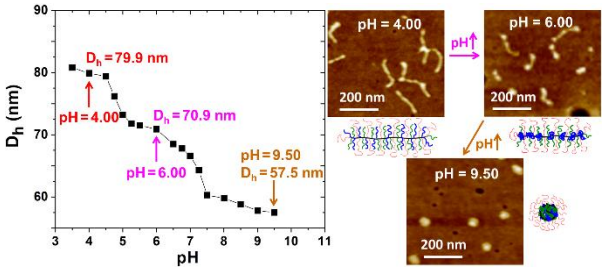

Abstract: Stepwise conformational transitions of molecular bottlebrushes (MBBs) from extended wormlike to partially collapsed and stable globular in aqueous solution were realized with the use of two distinct stimuli-responsive polymers and poly(ethylene oxide) (PEO) as the side chains, where PEO served as a stabilizer when the responsive side chains became insoluble. Three dually responsive brush polymers, composed of either two distinct pH-responsive or two different thermoresponsive or one pH- and one thermoresponsive polymers along with PEO randomly grafted on the backbone polymer, were synthesized by a click grafting to method. Dynamic light scattering studies showed that all three brush polymers displayed two successive steplike size transitions in aqueous solutions in response to application of external stimuli, with overall size

decreases of 27 – 29 %. ^{1}H NMR spectroscopy analysis confirmed that the size transitions of MBBs originated from the pH-induced soluble-to-insoluble and/or the temperature-triggered lower critical solution temperature transitions of responsive side chain polymers in the brushes. Atomic force microscopy revealed stepwise conformational changes from extended wormlike (with and without a pearl-necklace morphology) to partially collapsed (shrunken wormlike or wavelike or C-/S-shaped) and globular nano-objects stabilized by PEO side chains. As a demonstration of potential applications, Nile Red was encapsulated in the dually pH-responsive globular MBBs as a hydrophobic model drug and its stepwise release was achieved upon gradually decreasing pH.

Introduction

Molecular bottlebrushes (MBBs), also termed bottlebrush polymers, are a special type of graft copolymers in which relatively short polymer chains are covalently grafted on a long backbone polymer with a sufficiently high grafting density that the backbone is forced to take on stretched conformations.[1-6] These architecturally complex polymers have attracted considerable attention in the past years, and their potential applications have been demonstrated in a wide variety of areas, including drug delivery,[7,8] photonic crystals,[9-11] supersoft elastomers,[12] biological tissue-inspired advanced organic materials,[13] and surface coating for lubrication.[14] Due to the dense grafting of macromolecular side chains, MBBs exhibit many intriguing characteristics and behavior, including high persistence length, no backbone entanglement, large conformational changes (i.e., shape transitions), and unusual crystal habit.[1-6,15] Among these, stimuli-triggered shape transitions of MBBs are particularly interesting.[2,3,6] While bottlebrush polymers adopt a cylindrical or wormlike shape under conditions favorable for side chains (e.g., in good solvents), they can exhibit pronounced and abrupt shape changes and take on different conformations (e.g., spherical) when the interactions of the side chains with the environment become unfavorable. Shape-changing MBBs may find applications in areas such as delivery of substances, regulation of molecular interactions, and templated synthesis of nanomaterials with controlled morphologies.[6,8,16]

Stimuli-induced shape transitions of MBBs from wormlike to globular or from starlike to disklike were demonstrated at interfaces.[17-21] Sheiko and coworkers showed that linear and star MBBs with homografted poly(*n*-butyl acrylate) (P*n*BA) side chains underwent reversible rod-to-sphere and star-to-disk shape transitions, respectively, at the air-water interface by lateral compression and decompression.[17,18] MBBs with stimuli-responsive polymers as the side chains can undergo shape transitions in solution in response to environmental stimuli, which are more

relevant to potential applications. A variety of stimuli-responsive polymers, including thermosensitive water-soluble polymers, pH- and light-responsive polymers as well as polyelectrolytes, have been employed to construct stimuli-responsive MBBs.[6,16,22-36] Li et al. reported that thermosensitive MBBs with poly(*N*-isopropylacrylamide) (PNIPAm) side chains collapsed from a wormlike to a globule shape upon heating from below to above the lower critical solution temperature (LCST) of PNIPAm.[22] The collapsed globular PNIPAm MBBs, however, were unstable at high temperatures; the brush molecules were found to aggregate and eventually precipitate out from water. Polyelectrolyte MBBs can change their conformations in water in response to the addition of surfactants, salts, and oppositely charged polyelectrolytes.[28-31] For example, unusual helical conformations of MBBs with polyelectrolyte side chains were found in highly dilute aqueous solutions upon the addition of multivalent ions or surfactants.[28,29] Multiple wormlike-globular shape transitions for cationic MBBs with quaternary ammonium polyelectrolyte side chains in dilute aqueous solutions were observed when sodium dodecyl sulfate (SDS), β-cyclodextrin, and 1-adamantylammonium chloride were added sequentially into the solution.[30] However, at a slightly higher concentration (e.g., 1 mg/mL), the bottlebrush polymer precipitated out immediately after the addition of SDS.

The collapsed globular MBBs in solution can be stabilized against aggregation by introducing a second polymer into the side chains, either as a second set of side chains in heterografted brushes or as the outer block of block copolymer side chains in homografted MBBs.[6,8,16,37-44] When the responsive side chains or the inner blocks of bicomponent MBBs become insoluble in water, driving the shape transitions from worm- or starlike to globular, the second polymer in the side chains serves as a stabilizer. The resultant core-shell globular nano-objects are in fact unimolecular spherical micelles. If the binary heterografted brush polymers are composed of two distinct types

of stimuli-responsive polymeric side chains, two stable globular states with different polymers in the core can be obtained under different conditions.[40] Our bicomponent MBBs were synthesized by a grafting to method using the highly efficient copper(I)-catalyzed alkyne-azide cycloaddition (CuAAC) click reaction to graft alkyne-end-functionalized polymers onto an azide-functionalized backbone polymer.[6,16,37-42] This approach is modular,[8,16,37-42,45-50] allowing for separate synthesis and characterization of backbone and side chain polymers, simultaneous incorporation of different polymers into the side chains, and facile tuning of the molar ratios of different side chain polymers.

In the present work, we show that stepwise conformational transitions of linear MBBs from wormlike to partially collapsed and globular can be achieved with the use of two distinct stimuli-responsive polymers along with poly(ethylene oxide) (PEO) as the side chains. PEO is introduced to stabilize the brush molecules against aggregation when the responsive side chains become insoluble.[16] Three dually responsive linear ternary MBBs were constructed by the click grafting to method using thermosensitive poly(ethoxydi(ethylene glycol) acrylate) (PDEGEA) with an LCST of 9 °C,[51,52] thermosensitive poly(methoxydi(ethylene glycol) acrylate) (PDEGMA) with an LCST of 38 °C,[53] pH-responsive poly(2-(*N*,*N*-diethylamino)ethyl methacrylate) (PDEAEMA) with a pK_a of 7.4, and pH-responsive poly(2-(*N*,*N*-di(*n*-butyl)amino)ethyl methacrylate) (PDBAEMA) with a pK_a of 5.1,[54,55] along with 5 kDa PEO (Scheme 1). The three ternary MBB samples are: (i) MBB-PP composed of PEO and two pH-responsive polymers (PDEAEMA and PDBAEMA), (ii) MBB-TT consisting of PEO and two thermoresponsive polymers (PDEGEA and PDEGMA), and (iii) MBB-TP comprising PEO and two different stimuli-responsive polymers (PDEGEA and PDEAEMA) as the side chains, where T and P represent a thermosensitive and a pH-responsive polymer, respectively. The stimuli-induced conformational changes of these MBBs in aqueous solutions were studied by dynamic light scattering (DLS), ^{1}H NMR spectroscopy analysis, and

atomic force microscopy (AFM). In addition, as a demonstration of potential applications, MBB-PP was used to encapsulate Nile Red in the globular form, and stepwise release of this hydrophobic model drug from the collapsed globular brushes was achieved upon gradually decreasing pH.

Scheme 1. Synthesis of Dually Responsive Linear Ternary Heterografted Molecular Bottlebrushes, MBB-PP, -TT, and -TP, and Stimuli-Induced Stepwise Collapse in Aqueous Solution

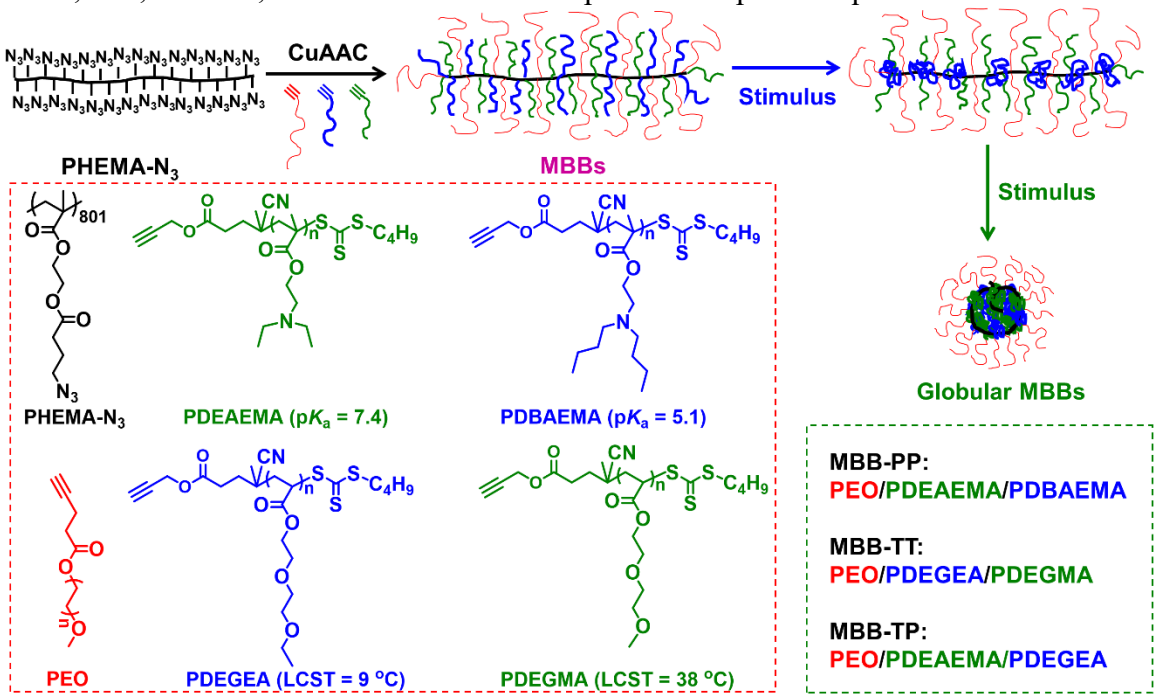

Results and Discussion

Synthesis and Characterization of Dually Responsive Ternary MBBs. Three linear MBBs composed of randomly grafted 5 kDa PEO and two stimuli-responsive polymers were prepared by a grafting-to approach via the CuAAC reaction (Scheme 1). This method is particularly suitable for the preparation of multicomponent brush polymers, which not only can produce high grafting density brushes but also allows for convenient tuning of the side chain composition. Stimuli-responsive alkyne-end-functionalized side chain polymers, PDEAEMA, PDBAEMA, PDEGEA, and PDEGMA (Scheme 1), were prepared by reversible addition-fragmentation chain transfer

(RAFT) polymerization[56] of respective monomers in anisole using an alkyne-functionalized trithiocarbonate compound (CTA-Alkyne, Figure S1) as the chain transfer agent and 2,2′-azobis(2-methylpropionitrile) as the initiator. The details can be found in the Supporting Information, and the characterization data for all side chain polymers are summarized in Table 1. Size exclusion chromatography (SEC) analysis showed that the dispersities (*Đ*) of these polymers were in the range of 1.12 to 1.16 with a unimodal peak (Figures S2-S6), indicating that the RAFT polymerizations were well controlled. The degrees of polymerization (DPs) of these polymers were in the range of 43 to 57, calculated from the monomer conversions determined by ^{1}H NMR spectroscopy analysis and the initial molar ratios. Alkyne-end-functionalized PEO was synthesized by reacting 5 kDa poly(ethylene oxide) monomethyl ether with 4-pentynoic acid using 1-(3-dimethylaminopropyl)-3-ethylcarbodiimide hydrochloride and 4-(dimethylamino)pyridine as the catalysts.[16] The linear azide-functionalized backbone polymer with a DP of 801 and a degree of azide functionalization of 96.7%, PHEMA-N_3, was prepared by atom transfer radical polymerization of 2-(trimethylsilyloxy)ethyl methacrylate and post-polymerization modifications, including the deprotection of trimethylsilyl groups, reaction with 4-bromobutyryl chloride, and substitution of pendant bromine atoms with azide, as described previously.[50]

Table 1. Characterization Data for Side Chain Polymers Used for Synthesizing MBBs

Side Chain Polymer	Molecular Weight	*Đ*	DP
PEO	M_n = 5 kDa [a]	1.04 [b]	114 [c]
PDEAEMA-45	$M_{n,SEC}$ = 6.9 kDa [d]	1.14 [d]	45 [e]
PDEAEMA-56	$M_{n,SEC}$ = 7.8 kDa [d]	1.14 [d]	56 [e]
PDBAEMA	$M_{n,SEC}$ = 9.9 kDa [d]	1.12 [d]	43 [e]
PDEGEA	$M_{n,SEC}$ = 10.3 kDa [d]	1.16 [d]	57 [e]
PDEGMA	$M_{n,SEC}$ = 9.3 kDa [d]	1.15 [d]	55 [e]

[a] Molecular weight from the vendor. [b] Dispersity (*Đ*) was determined by a PL-GPC 20 system relative to polystyrene standards. [c] Degree of polymerization (DP) was calculated from the M_n. [d] Number-average molecular weight ($M_{n,SEC}$) and *Đ* were determined using a PL-GPC 20 system relative to polystyrene standards. [e] Calculated from the initial monomer-to-CTA molar ratio and the monomer conversion.

The click reactions for the synthesis of the three brush polymers were carried out in tetrahydrofuran (THF) at ambient temperature using CuCl and *N*,*N*,*N*′,*N*″,*N*‴-pentamethyldiethylenetriamine as the catalyst and ligand, respectively. In order to achieve high grafting density MBBs, excess side chain polymers were employed with a feed molar ratio of ~ 1.5 : 1 for the side chain polymers to the azide groups. At the end of the click reaction, benzyl propargyl ether was added to cap the possible remaining unreacted azide groups on the backbone to mitigate potential issues in the subsequent purification and study. The MBBs were purified by a combination of precipitation/fractionation and centrifugal filtration using an Amicon 50 kDa MWCO filter. The complete removal of excess side chain polymers from the MBBs was confirmed by SEC analysis (Figures S7-S9), and ^{1}H NMR analysis showed that the molar ratios of different side chain polymers in the purified brushes were similar to the feed ratios. Using the SEC peak area percentages of the brushes and the unreacted side chain polymers in the final reaction mixture and the side chain composition from ^{1}H NMR analysis along with the feed masses and the DPs of the side chain polymers, the grafting densities of MBB-TT and MBB-TP were estimated to be 93.0% and 90.4%, respectively. The absolute $M_{w,expt}$ values of these two brush polymers measured by a SEC-multiangle light scattering (SEC-MALS) system were 7.92×10^6 Da and 7.81×10^6 Da, respectively, which were close to the calculated $M_{w,calc}$ values, 7.51×10^6 Da and 7.29×10^6 Da, based on the grafting densities and the calculated $M_{w,calc}$ values of the backbone and the side chain polymers (M_n calculated from DP × $Đ$). The grafting density of MBB-PP, however, could not be estimated by the above method because PDBAEMA was insoluble in DMF. SEC-MALS analysis of purified MBB-PP in DMF, prepared by gradually adding DMF into a dilute THF solution of MBB-PP and then evaporating the solvents to an appropriate concentration, showed that the $M_{w,expt}$ of MBB-PP was 7.13×10^6 Da (Figure S10), similar to the $M_{w,expt}$ values of MBB-TP and -TT.

This $M_{w,expt}$, however, is higher than the calculated $M_{w,calc}$ value for a hypothetical brush polymer with the same side chain composition and a full grafting density (i.e., 96.7% - the degree of azide functionalization) ($M_{w,calc} = 6.38 \times 10^6$ Da, see the Supporting Information), which could be due to the loss of lower molecular weight brush molecules during the purification. The characterization data for the three bottlebrush polymers are summarized in Table 2 along with the aforementioned calculated values.

Table 2. Characterization Data and Calculated Values for MBBs

MBBs	Side Chain Polymer 1 and Molar Percentage [a]	Side Chain Polymer 2 and Molar Percentage [a]	Side Chain Polymer 3 and Molar Percentage [a]	Grafting Density [b]	$M_{w,expt.}$ [c] (Da)	$M_{w,calc.}$ [d] (Da)
MBB-PP	PEO, 51.0%	PDEAEMA-45, 29.2%	PDBAEMA, 19.8%	NA	7.13×10^6	6.38×10^6 (for a grafting density of 96.7%)
MBB-TT	PEO, 34.4%	PDEGEA, 32.9%	PDEGMA, 32.7%	93.0%	7.92×10^6	7.51×10^6
MBB-TP	PEO, 40.4%	PDEGEA, 32.2%	PDEAEMA-56, 27.4%	90.4%	7.81×10^6	7.29×10^6

[a] Molar percentages of side chain polymers of MBBs were determined by ^{1}H NMR analysis. [b] Grafting density was estimated using the SEC data, feed masses, and side chain composition. [c] Experimental absolute M_w ($M_{w,expt}$) was measured using a SEC-MALS system. [d] Calculated absolute M_w ($M_{w,calc}$) was obtained by considering the M_w values of the azide-carrying backbone and side chain polymers, calculated from DPs and dispersities ($M_{n,calc} \times Đ$), and the grafting density.

pH-Induced Stepwise Conformational Transitions of MBB-PP in Aqueous Solution. MBB-PP is composed of 51.0 mol% PEO and two different pH-responsive polymers, 29.2 mol% PDEAEMA-45 (DP = 45) with a pK_a of 7.4 and 19.8 mol% PDBAEMA with a pK_a of 5.1,[54,55] densely and randomly grafted on the backbone polymer as the side chains. The two tertiary-amine-containing polymethacrylates are insoluble in water at pH > pK_a and undergo soluble-insoluble transitions in different pH ranges. Figure 1A shows the plot of the apparent hydrodynamic diameter (D_h) of 0.2 mg/g MBB-PP in a 25 mM phosphate buffer at 25 °C versus pH. At pH = 3.50, the D_h

was 80.8 nm. Upon increasing pH, two steplike size-reduction transitions were observed. The first one occurred in the pH range of 4.50 (D_h = 79.4 nm) to 5.26 (D_h = 71.8 nm), around the pK_a of PDBAEMA, which was attributed to the collapse of PDBAEMA side chains caused by the deprotonation of the pendant charged di(*n*-butyl)aminoethyl groups. This was followed by a plateau in the pH range from ~5.3 to ~6.0, where the size decreased only slightly. The second transition was observed at pH = ~7.0; the D_h decreased from 68.5 nm at pH = 6.50 to 60.3 nm at pH = 7.50 and leveled off to 57.5 nm at pH = 9.50. The overall size change from pH 3.50 to 9.50 was 23.3 nm (~29%), i.e., the hydrodynamic volume decreased by 64.0%. The size transitions were reversible; decreasing the pH to 8.00, 5.98, and 4.00 resulted in D_h values right on the curve (Figure 1A). Throughout the processes of changing pH, the hydrodynamic size distributions were unimodal and narrow as can be seen from the three curves shown in the inset of Figure 1A. We note here that without PEO as a stabilizer, MBBs with homografted PDEAEMA side chains precipitated out immediately at pH > pK_a.[39]

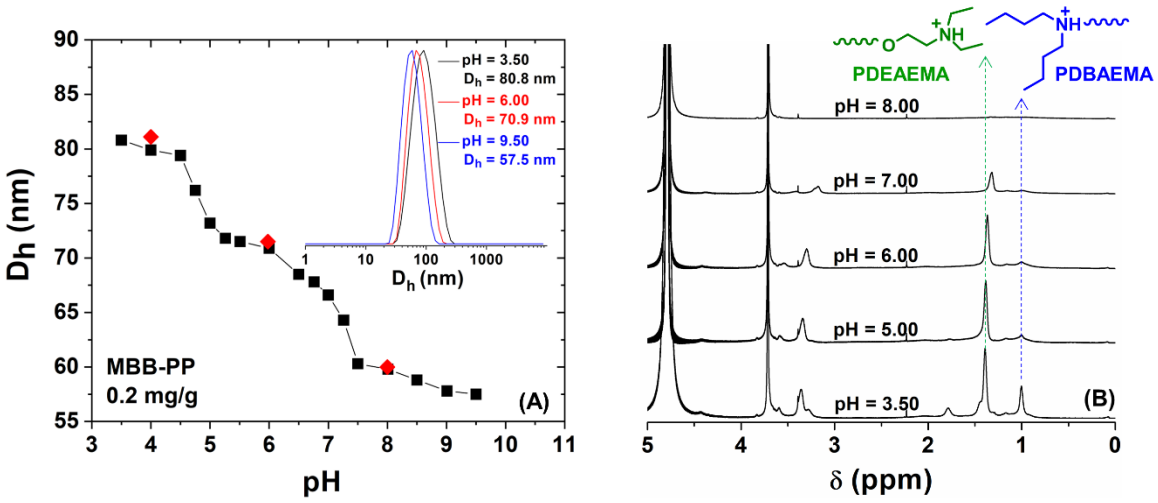

Figure 1. (A) Apparent hydrodynamic diameter (D_h) of 0.2 mg/g MBB-PP in a 25 mM phosphate buffer at 25 °C upon increasing pH. The three red diamond data points were collected from the process of decreasing pH from pH = 9.50. The inset shows hydrodynamic size distributions of MBB-PP at pH values of 3.50, 6.00, and 9.50. (B) ^{1}H NMR spectra of 4.0 mg/g MBB-PP in a 10 mM phosphate buffer prepared using D_2O at various pH values. The ^{1}H NMR spectra were normalized against the HDO peak at 4.79 ppm.

^{1}H NMR spectroscopy analysis was employed to confirm that the steplike size transitions observed from DLS measurements were driven by the solubility changes of the two pH-responsive side chain polymers. As shown in Figure 1B, the peak of -$CH_2CH_2CH_2CH_3$ from PDBAEMA at ~1.0 ppm was visible at pH 3.50 but nearly disappeared at pH 5.00, which matched the first transition observed by DLS (Figure 1A). Note that the disappearance or the decrease in intensity of the peak in the NMR spectra is caused by the loss of mobility.[40] With further increasing pH, the peak of -CH_2CH_3 from PDEAEMA at ~ 1.4 ppm decreased significantly in intensity at pH = 7.00 and completely disappeared at pH = 8.00, corresponding to the second size reduction transition from DLS measurements.

AFM was performed to study the morphologies of the brushes at different pH values. The samples were prepared by spin casting the phosphate buffer solutions of 0.050 mg/g MBB-PP at pH 4.00, 6.00, and 9.50 on PMMA-coated mica disks at room temperature. At pH = 4.00, MBB-PP assumed wormlike conformations with a pearl-necklace morphology comprising a string of beads along the backbone (Figures 2A and S11). The height, length, and width of a representative bead marked by an arrow in Figure 2A were 3.0, 23.7, 19.1 nm, respectively. Image analysis showed that the average length of 131 brush molecules was 171.1 ± 42.6 nm, which represents a degree of stretching of 85% considering the maximum length of the brushes with a backbone DP of 801. The high degree of stretching can be attributed to the electrostatic repulsive interactions between protonated side chains. The pearl-necklace morphology presumably resulted from the microphase separation between protonated PDEAEMA and PDBAEMA and neutral PEO side chains. Similar pearl-necklace morphologies were reported in the literature for bicomponent MBBs, either with homografted core-shell diblock copolymer side chains or heterografted two distinct homopolymer side chains,[40,50,57,58] and we are not aware of MBBs with one-component

homopolymer side chains exhibiting such a morphology. When the solution pH was raised to 6.00 at which PDBAEMA side chains became insoluble in water and PDEAEMA was still protonated, the pearl-necklace morphology was maintained for longer brush molecules, whereas shorter brushes appeared to transform into a roughly globular or short rodlike shape (Figures 2B and S12). The height, length, and width of the representative bead marked with an arrow in Figure 2B were slightly larger (3.8, 25.4, and 25.1 nm, respectively). The average length of 144 brush molecules was 110.9 nm ± 44.3 nm, significantly shorter than that at pH = 4.00 (171.1 ± 42.6 nm) due to the collapse of PDBAEMA side chains. Further increasing the pH to 9.50 caused all of the brushes to collapse into globules (Figures 2C and S13), with an average diameter of 48.9 ± 9.3 nm from the measurements of 75 MBB molecules (two measurements for each in perpendicular directions) and a representative height of 5 nm. The results from the AFM study were consistent with the large size drops observed from the DLS study when the pH was increased from 4.00 (D_h = 79.9 nm) to 6.00 (70.9 nm) and 9.50 (D_h = 57.5 nm). Note that even when the height of globular MBB-PP brushes at pH = 9.50 from the AFM study was ~ 5 nm, the average diameter (48.9 nm) was still smaller than the D_h from the DLS measurements (57.5 nm); we believe that this is because the hydrophilic 5 kDa PEO side chains remained well solvated in the solution. We also note here that the morphologies of MBBs observed by AFM in the dry state can be different from those in the solutions. Nevertheless, all the AFM samples were prepared on PMMA-coated mica using the same spin-casting process.

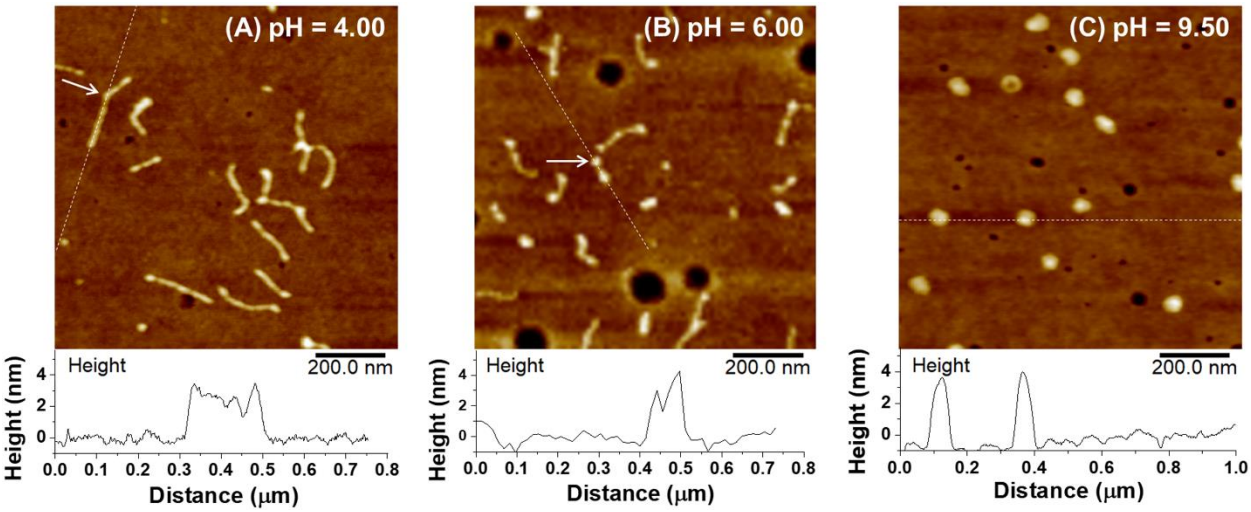

Figure 2. AFM height images of MBB-PP spin cast on PMMA-coated mica from a 0.050 mg/g solution of MBB-PP in a 10 mM phosphate buffer with a pH of 4.00 (A), 6.00 (B), and 9.50 (C). The plot in the bottom of each image shows the cross-sectional profile along the dashed line.

Temperature-Induced Stepwise Conformational Transitions of MBB-TT in Aqueous Solution. MBB-TT contained two thermoresponsive polymers, 32.9 mol% PDEGEA with an LCST of 9 °C and 32.7 mol% PDEGMA with an LCST of 38 °C, in the side chains along with 34.4 mol% PEO. Unlike MBB-PP, where stepwise conformational changes were induced through the addition of a basic or an acidic solution to adjust the pH, MBB-TT represents an opportunity to realize stepwise collapse of side chains solely by changing temperature. Figure 3A shows the D_h of MBB-TT in Milli-Q water at a concentration of 1.0 mg/g as a function of temperature upon heating from 1 °C to 65 °C from DLS measurements. When the temperature was 1 °C, the D_h of MBB-TT was 66.7 nm. With increasing temperature, two size transitions were observed; the first one began at 10 °C, around the LCST of PDEGEA, and continued over a temperature range of ~10 °C, where the D_h decreased from 65.0 nm at 10 °C to 56.3 nm at 22 °C. In the following temperature range of 22 to 37 °C, the D_h exhibited little changes. The second steplike size transition occurred in the temperature range of 37 to 52 °C, with an onset temperature of 37 °C, close to the LCST of PDEGMA. The D_h decreased from 55.1 nm at 37 °C to 49.3 nm at 52 °C and then leveled

off above 52 °C, reaching 47.6 nm at 65 °C. Again, a single narrow size distribution was observed at each selected temperature (see the three hydrodynamic size distributions at 1, 25, and 65 °C in the inset of Figure 3A). We note here that the D_h values of MBB-TT at two different concentrations, 1.0 and 0.2 mg/g, at 1 °C, were essentially the same, and so were the D_h values at 65 °C (Figure S14), suggesting unimolecular collapse of MBB-TT at the concentration of 1.0 mg/g upon heating.

Variable temperature ^{1}H NMR spectroscopy was performed to study the LCST transitions of the two thermoresponsive side chain polymers in MBB-TT upon heating, which are presumably responsible for the stepwise size transitions in Figure 3A. Figure 3B and C shows the ^{1}H NMR spectra of MBB-TT in D_2O at a concentration of 4.0 mg/g in the temperature ranges of 5 to 20 °C and 35 to 50 °C, respectively. Upon heating from 10 to 15 °C, the peak at ~1.0 ppm, which is from the -OCH_2CH_3 of PDEGEA, decreased and broaden slightly (Figure 3B). This temperature-induced change was much less pronounced than the pH-induced soluble-to-insoluble transitions of PDEAEMA and PDBAEMA side chains in MBB-PP (Figure 1B). This could be attributed to (i) the nature of the liquid-liquid phase separation of thermosensitive polymers in water above the LCSTs[59,60] and (ii) the influence of the strongly hydrated PEO and PDEGMA side chains.[40] For PDEGMA side chains, upon heating from 35 to 50 °C, the peak at 3.50 ppm (-$OCH_2CH_2OCH_3$) decreased noticeably, consistent with the expected LCST transition of PDEGMA.

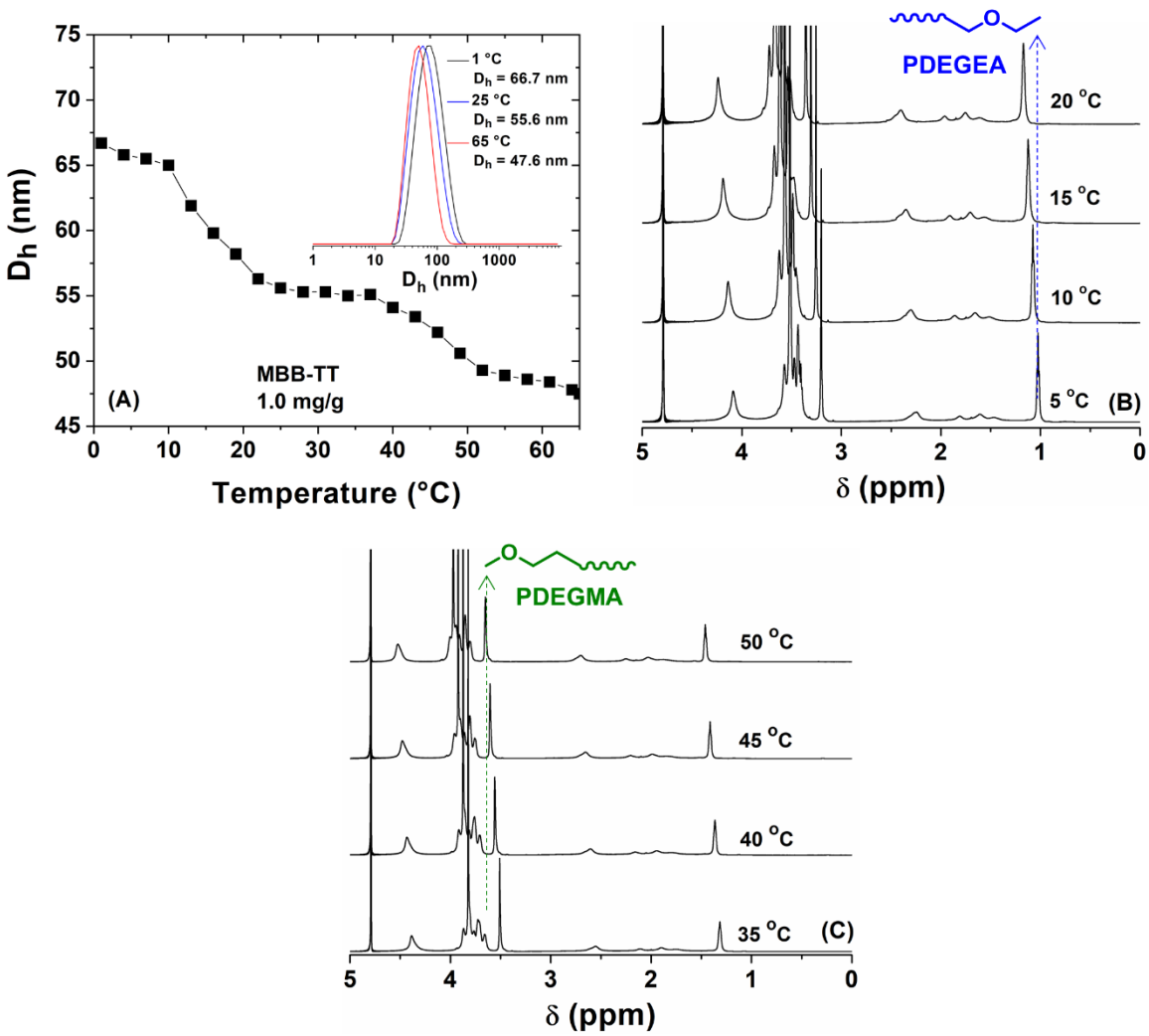

Figure 3. (A) Plot of D_h of 1.0 mg/g MBB-TT in Milli-Q water versus temperature in a heating process from a DLS study. The inset shows hydrodynamic size distributions at 1, 25, and 65 °C, and variable temperature ^{1}H NMR spectra of MBB-TT in D_2O with a concentration of 4.0 mg/g in the temperature ranges of 5 to 20 °C (B) and of 35 to 50 °C (C). The ^{1}H NMR spectra were normalized again the HDO peak at 4.79 ppm.

AFM showed that MBB-TT brushes spin cast on PMMA-coated mica at 0 °C were wormlike (Figures 4 and S15). The average length of 106 MBB brush molecules was 169.2 ± 37.5 nm, and the typical height was ~1 nm (see the cross-sectional profile at the bottom of Figure 4A). When the temperature was raised to 30 °C, the brushes shrank noticeably (Figures 4B and S16). Interestingly, longer brushes took on wavelike conformations, while short ones assumed C or S shapes, which is likely due to the requirement for locally collapsed and aggregated PDEGEA side

chains to minimize the contact with water along the backbone under the conditions that PEO and PDEGMA are still highly hydrated. Note that C- and S-shaped brush molecules were previously reported in the literature for P*n*BA MBBs at the air-water interface after lateral decompression and were theoretically explained as that the uneven distribution of side chains on the two sides of the backbone resulted in a decrease of the elastic energy of the side chains.[17,61] The brush height was ~2.5 nm, in contrast to ~1 nm at 0 °C, and the average cross-length (from one side to another) of 152 MBB molecules from image analysis was 124.8 ± 42.4 nm. Further heating to 65 °C, the brushes were found to be mostly globular (Figures 4C and S17), though some molecules appeared to be unfolded on the substrate, which could be due to the shearing force in the sample preparation process. The average dimension of 66 globular MBB brushes (two measurements for each in perpendicular directions) was 52.1 ± 15.2 nm, and the typical height was ~ 4 nm. Thus, the results from AFM analysis agreed with the DLS data (Figure 3A).

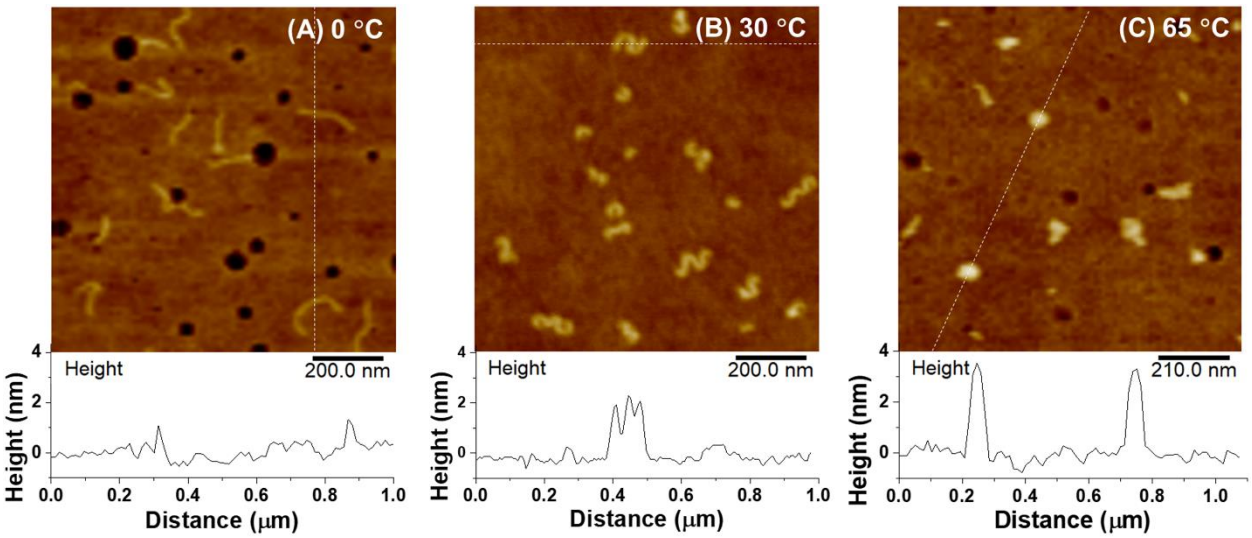

Figure 4. AFM height images of MBB-TT spin cast on PMMA-coated mica from a 0.050 mg/g solution of MBB-PP in Milli-Q water at T = 0 °C (A), 30 °C (B), and 65 °C (C). The plot in the bottom of each image shows the cross-sectional profile along the dashed line.

pH- and Temperature-Induced Stepwise Conformational Changes of MBB-TP in Aqueous Solution. MBB-TP comprised 32.2 mol% thermoresponsive PDEGEA, 27.4 mol% pH-responsive PDEAEMA-56 (DP = 56), and 40.4 mol% PEO side chains. The stepwise collapse of stimuli-responsive side chains in this brush polymer can be induced through two routes: (i) increasing pH from below to above the pK_a of PDEAEMA at a temperature below the LCST of PDEGEA, followed by heating to collapse the thermoresponsive side chains; (ii) raising temperature across the LCST of PDEGEA while PDEAEMA side chains are protonated, following by changing the pH from below to above the pK_a of PDEAEMA. Figure 5 shows the DLS results for route (i). A 1.0 mg/g solution of MBB-TP in a 10 mM phosphate buffer with a pH of 5.00 was prepared in an ice/water bath, and the D_h at 1 °C was found to be 72.9 nm. With increasing pH to 8.00 at 1 °C, the D_h decreased slightly to 70.5 nm, followed by a sharp drop to 60.5 nm at pH = 8.90, beyond which the size levelled off. The overall size reduction from pH 5.00 to 9.50 was 12.9 nm (~ 18%). We previously observed that for pH-induced full collapse of binary MBBs (i.e., from wormlike/starlike to globular) the size decreased by ~ 30%.[39,40] Thus, the overall decrease in the D_h of MBB-TP here implied partial collapse of the brushes. The pH-induced shrinking of MBB-TP was reversible upon lowering pH, as can be seen from the red circles in Figure 5A. Similar to MBB-PP, the hydrodynamic size distributions of MBB-TP remained narrow and unimodal throughout the pH-changing process, suggesting unimolecular collapse. Note that the pH-induced size transition of MBB-TP at 1 °C occurred in the pH range of 8.00 to 8.90, with the mid-point at pH = 8.45, much higher than the reported pK_a of PDEAEMA.[54,55] This is different from the observation for PDEAEMA side chains of MBB-PP at 25 °C in Figure 1A, but similar to our previous report for binary heterografted three-arm star MBBs,[40] which exhibited a sharp size decrease at pH = ~ 8.1 at 1 °C. The delayed size transition can be attributed to two factors. (i) The

pH values were measured in an ice/water bath, whereas the pK_a values are usually determined at 25 °C or ambient temperature. We calibrated the pH meter at 0 °C using pH = 4.01, 7.00, and 10.01 standard buffer solutions, whose pH values at 0 °C were 4.00, 7.11 and 10.32, slightly different from the values at 25 °C. (ii) Figure 5A shows the D_h values of MBB-TP upon increasing pH, not the solubility change of PDEAEMA side chains. The fully hydrated PEO and PDEGEA side chains of MBB-TP at 1 °C were believed to keep the brushes in the wormlike state to higher pH values above the pK_a of PDEAEMA until more monomer units were deprotonated to drive the shrinking of MBB-TP. As a result, the size reduction transition was delayed to a slightly higher pH range.

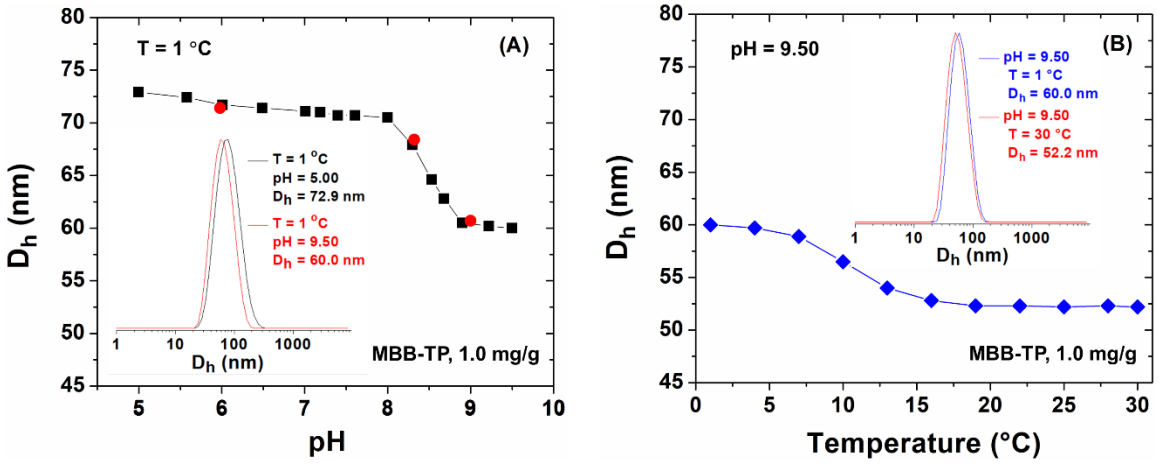

Figure 5. (A) Plot of D_h of 1.0 mg/g MBB-TP in a 10 mM phosphate buffer at 1 °C versus pH from DLS measurements. The inset shows the hydrodynamic size distributions of MBB-TP at T = 1 °C and two pH values (5.00 and 9.50). (B) Plot of D_h of 1.0 mg/g MBB-TP in a 10 mM phosphate buffer at pH = 9.50 versus temperature. The inset shows the hydrodynamic size distributions of MBB-TP at pH = 9.50 and two different temperatures (1 and 30 °C).

The sample was then gradually heated at pH = 9.50; the D_h exhibited a second size reduction transition, from 58.9 nm at 7 °C to 54.0 nm at 13 °C (Figure 5B), above which the D_h decreased slightly and reached 52.2 nm at 30 °C. The temperature-triggered size transition occurred at ~10 °C, almost the same as the reported LCST of PDEGEA (~9 °C). The overall decrease of D_h was

20.7 nm (~28%), from 72.9 nm at T = 1 °C and pH = 5.00 to 52.2 nm at T = 30 °C and pH = 9.50, corresponding to a hydrodynamic volume reduction by 63.3%. This indicated that the brushes likely fully collapsed at T = 30 °C and pH = 9.50. The single narrow size distributions shown in Figure 5B suggested that the brushes remained molecularly dispersed thanks to the steric stabilization provided by the PEO side chains.

Figure 6 shows the DLS results for the second route, that is, heating at a lower pH from below to above the LCST of PDEGEA and then increasing the pH from below to above the pK_a of PDEAEMA. At pH = 5.00, PDEAEMA side chains of MBB-TP were fully protonated and strongly hydrated, and only a small size decrease, yet appreciable, was observed upon heating, from 73.1 nm at 1 °C to 67.8 nm at 16 °C (Figure 6A). The transition occurred in a temperature range similar to that in Figure 5B, but the magnitude was smaller, only 3.6 nm from 7 to 16 °C, in contrast to 6.1 nm in Figure 5B in the same temperature range. This smaller D_h change was presumably caused by the highly hydrated protonated PDEAEMA side chains along with PEO side chains that kept the brushes in the wormlike form despite the temperature-induced collapse of PDEGEA side chains. At 19 °C, the pH of the solution was then gradually increased, and a large drop in D_h, ~13 nm, was observed in the pH range around the pK_a of PDEAEMA (Figure 6B). Above pH = 8.0, the D_h decreased only slightly and reached 53.4 nm at pH = 9.50. This D_h value is similar to that at the end of the first route (52.2 nm at T = 30 °C and pH = 9.50), also suggesting that the brushes were likely fully collapsed. The overall size reduction of MBB-TP in route (ii) was 19.7 nm (i.e., ~27%). Similarly, the pH-induced size transition was reversible with negligible hysteresis, as can be seen from the red circles in Figure 6B from decreasing pH, which fell right on the curve obtained from the process of increasing pH.

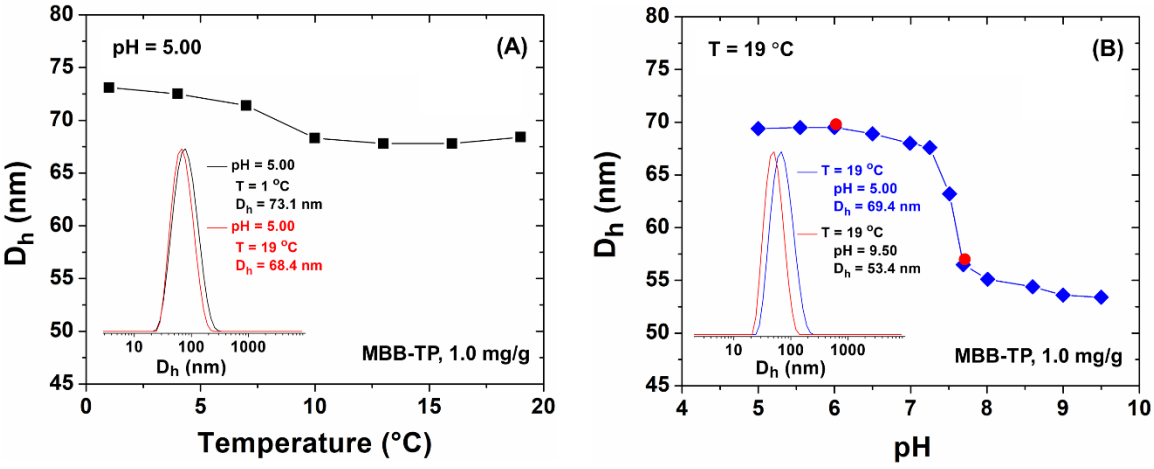

Figure 6. (A) Plot of D_h of 1.0 mg/g MBB-TP in a 10 mM phosphate buffer at pH = 5.00 versus temperature from DLS measurements upon heating. The inset shows the hydrodynamic size distributions of MBB-TP at pH = 5.00 and two temperatures (T = 1 and 19 °C). (B) Plot of D_h of 1.0 mg/g MBB-TP in a 10 mM phosphate buffer at T = 19 °C versus pH. The inset shows the hydrodynamic size distributions of MBB-TP at T = 19 °C and two pH values (5.00 and 9.50).

The observed stepwise side transitions originated from the collapse of PDEGEA and PDEAEMA side chains of MBB-TP in water in response to heating and pH increases, respectively, which were verified by ^{1}H NMR analysis of MBB-TP following the changes in both routes. Figure 7A shows the ^{1}H NMR spectra of MBB-TP in a 10 mM phosphate buffer prepared with D_2O at 4 °C with increasing pH from 5.00 to 9.50; clearly, the peak at 1.2 ppm, which was from -$HN^+(CH_2C\mathit{H}_3)_2$ of PDEAEMA side chains and visible at pH 5.00 to 7.50, completely disappeared at pH = 8.00 and 9.50. It was interesting to observe that the same peak almost disappeared at pH = 7.00 for MBB-PP in Figure 1B but still visible at pH = 7.50 for MBB-TP here, which could be caused by the temperature effect as discussed earlier. Note that the DLS measurements showed that the size transition began at pH = 8.00 at 1 °C and continued till about 8.90 (Figure 5A). This is likely because slightly higher pH might be necessary to drive the decrease in D_h, while the NMR signal reflects the mobility of the group. Figure 7B shows the variable temperature ^{1}H NMR spectra obtained at pH = 9.50 upon heating from 4 to 16 °C. The peak of -$OCH_2C\mathit{H}_3$ from

PDEGEA decreased significantly, with the transition occurring at ~10 °C, consistent with the LCST of PDEGEA. In the 2nd route, at pH = 5.00, the peak of -OCH_2CH_3 from PDEGEA decreased only slightly upon heating from 7 to 10 °C (Figure 7C) due to the protonated PDEAEMA side chains as discussed earlier for the observation in Figure 6A. At 25 °C, the peak of -$HN^+(CH_2CH_3)_2$ of PDEAEMA at 1.2 ppm completely disappeared at pH = 8.00 (Figure 7D); interestingly, the peak of -OCH_2CH_3 of PDEGEA at ~1.1 ppm became smaller noticeably, indicating the effects of the protonated and deprotonated PDEAEMA side chains on the signal of PDEGEA.

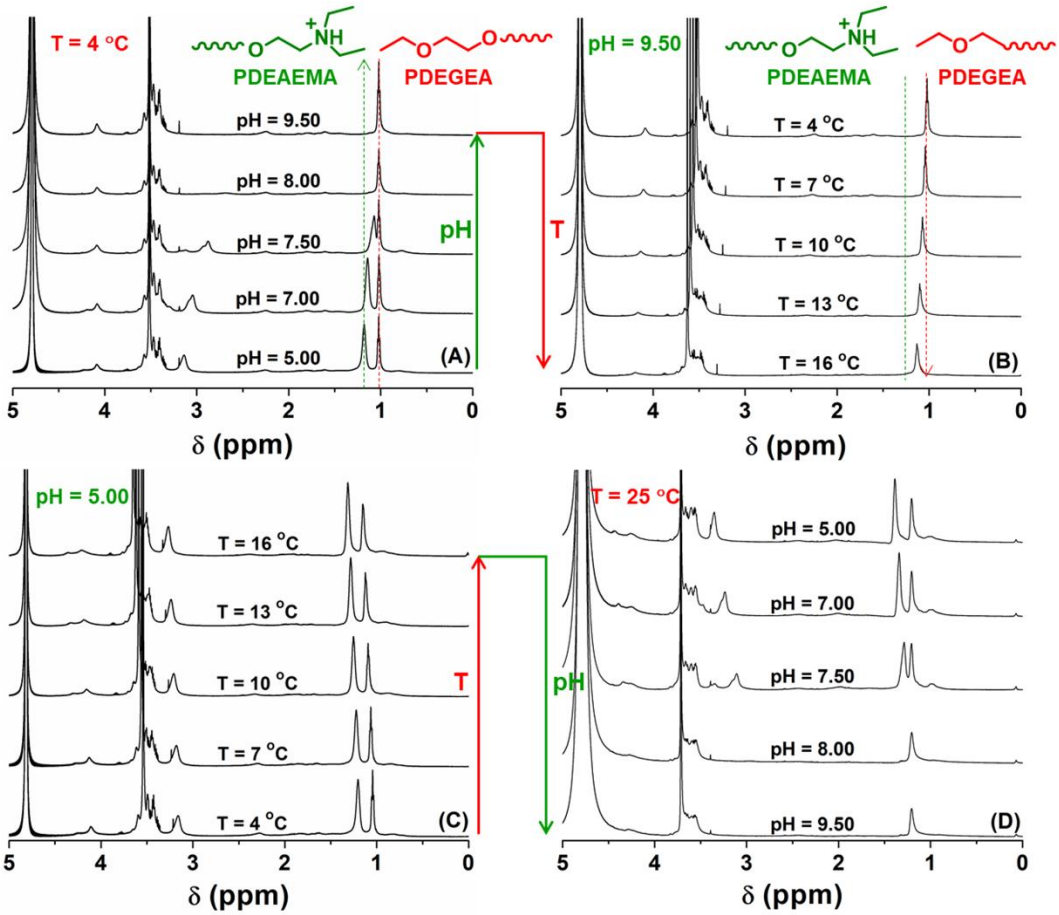

Figure 7. ^{1}H NMR spectra of a 4.0 mg/g solution of MBB-TP in a 10 mM phosphate buffer made with D_2O at 4 °C with increasing pH value from 5.00 to 9.50 (A), at pH = 9.50 with increasing temperature from 4 to 16 °C (B), at pH = 5.00 and various temperatures upon heating (C), and at 25 °C with increasing pH value from 5.00 to 9.50 (D). The ^{1}H NMR spectra were normalized against the HDO peak at 4.79 ppm.

To visualize the changes of MBB-TP under different conditions, AFM was performed. The AFM samples were prepared by spin casting 0.05 mg/g brush solutions on PMMA-coated mica disks immediately after the equilibration of the brush solutions, mica disks, and the spin stage of the spin coater at desired temperatures. Figure 8 shows the AFM height images of MPP-TP at different temperatures and pH values from both routes. At T = 0 °C and pH = 5.00, the brushes assumed a wormlike conformation with a pearl-necklace nanostructure composed of a number of beads (Figures 8A and S18), similar to but more pronounced than the morphology of MBB-PP at pH = 4.00 in Figure 2A. The representative bead marked with an arrow in Figure 8A had a length of 19.4 nm (along the backbone), a width of 12.9 nm, and a height of 3.7 nm. The height of the brushes showed undulations of ~1 nm, as can be seen from the cross-sectional profile at the bottom of Figure 8A. This peculiar morphology is also believed to be a result of microphase separation between the charged PDEAEMA side chains and the neutral PEO and PDEGEA side chains. The average length of 142 MBB molecules was 179.5 ± 41.7 nm, representing a degree of stretching of 89%. Upon increasing pH to 9.50 at 0 °C, the PDEAEMA side chains were deprotonated, and AFM imaging showed that height variations along the backbone were significantly smaller (< 0.5 nm) (Figures 8B and S19), although beadlike nanostructures were still visible. This observation suggested that the microphase separation of the side chains along the backbone were significantly weakened upon increasing pH to deprotonate the charged PDEAEMA side chains. Analysis showed that the average length of 246 brushes was 160.8 ± 40.7 nm, which was slightly shorter than that at pH = 5.00 and T = 0 °C (179.5 ± 41.7 nm). When the temperature was raised to 20 °C at pH 9.50, the brushes collapsed into a roughly globular shape, with a folded backbone being clearly visible for many globules in Figures 8C and S20. The typical height of folded brushes was

~4 nm, and the average diameter from the image analysis of 100 globular molecules (two measurements for each in perpendicular directions) was 54.5 ± 9.7 nm.

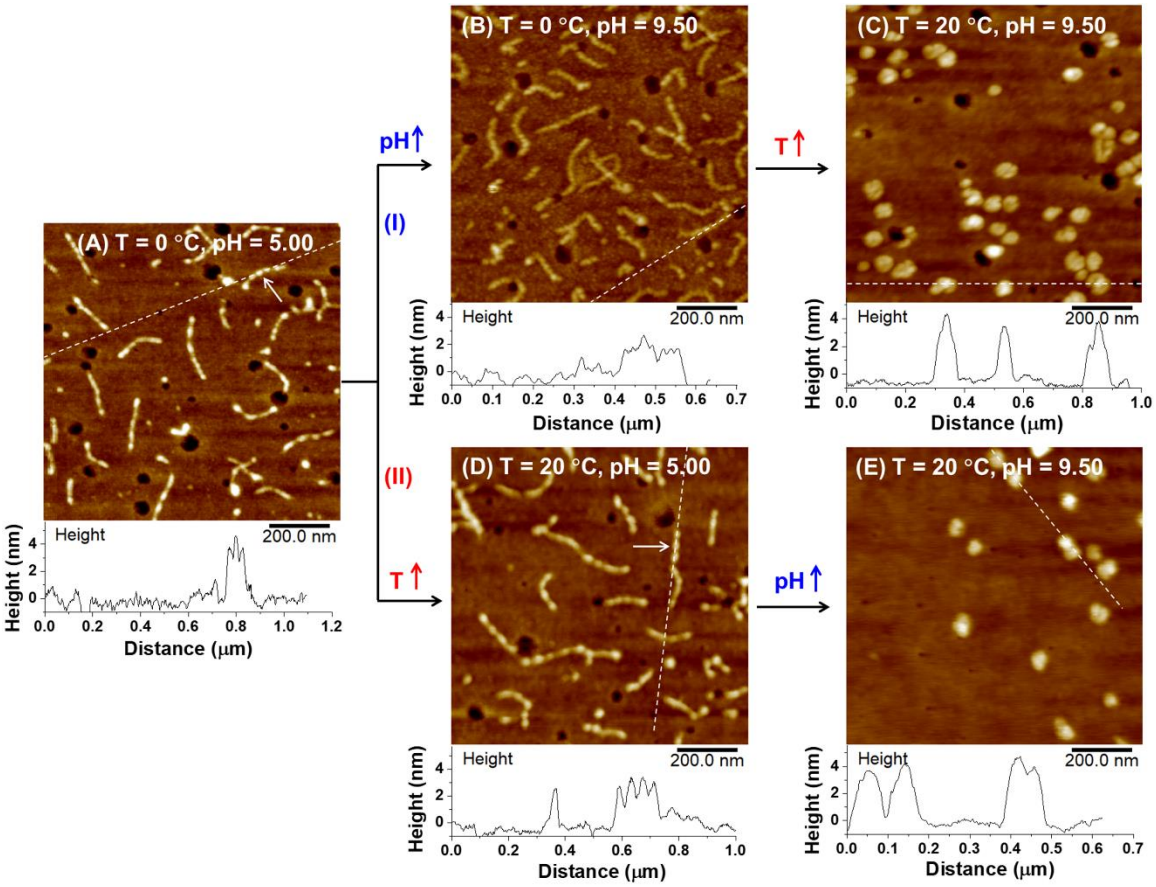

Figure 8. AFM height images of MBB-TP spin cast on PMMA-coated mica from a 0.050 mg/g solution of MBB-TP in a 5 mM phosphate buffer at T = 0 °C and pH = 5.00 (A), T = 0 °C and pH = 9.50 (C), T = 20 °C and pH = 9.50 (C), T = 20 °C and pH = 5.00 (D), and T = 20 °C and pH = 9.50 (E). The plot in the bottom of each AFM micrograph shows the cross-sectional profile along the dashed line in the height image.

When the MBB-TP solution with a pH of 5.00 was heated from 0 to 20 °C, AFM showed that the pronounced pearl-necklace morphology was maintained (Figures 8D and S21), with the typical bead (marked with an arrow) of a similar height (3.4 nm), a slightly larger length (26.4 nm) and width (21.3 nm) than the bead in Figure 8A. Image analysis showed that the average length of 211 brush molecules was 167.1 nm ± 36.4 nm, slightly shorter that at the conditions of pH = 5.00 and

T = 0 °C (179.5 ± 41.7 nm). This suggests that the heating-induced collapse of PDEGEA at pH = 5.00 had a rather small influence on the overall conformation and the pearl-necklace morphology of the brushes, consistent with the small changes in the D_h from DLS (Figure 6A) and in the intensity of the characteristic peak from ^{1}H NMR analysis (Figure 7C), which could be attributed to the strong hydration of PEO and protonated PDEAEMA side chains. Nevertheless, the collapse of PDEGEA side chains enhanced the microphase separation along the backbone as reflected by the larger beads in the pearl-necklace nanostructures in Figure 8D.

When the pH was increased from 5.00 to 9.50 at 20 °C, both responsive side chain polymers collapsed as can be seen from the ^{1}H NMR spectrum in Figure 7D, the brushes transformed into a globular shape stabilized by PEO side chains (Figures 8E and S22); the typical height was ~ 4-5 nm, similar to the collapsed brushes shown in Figure 8C. The average diameter of 93 globular brushes measured (two measurements for each in perpendicular directions) was 51.8 ± 9.9 nm, slightly smaller than the average size of the globular brushes from the first route (54.5 ± 9.7 nm), likely because the brushes in Figure 8C appeared to spread slightly on the surface. Thus, studies by DLS, NMR, and AFM showed that MBB-TP exhibited stepwise collapse of side chains in response to external stimuli and eventually transformed into globular shapes stabilized by the PEO side chains. Subtle differences were observed from different routes for the stepwise conformational transitions of MBB-TP in aqueous solutions.

Stepwise Release of Hydrophobic Model Drug, Nile Red, from Collapsed Globular MBB-PP. Shape-changing MBBs have potential application in many areas, including manipulation of molecular interactions, delivery of substances, and templated synthesis of inorganic nanoparticles of different morphologies via shape transitions. In particular, ternary MBBs with two distinct stimuli-responsive polymers in the side chains provide a unique opportunity to achieve stepwise

release of hydrophobic substances encapsulated in the globular brushes. Nile Red is commonly used as a hydrophobic fluorescence probe for study of block copolymer micellization in water because its fluorescence is negligible in water but increases significantly in the hydrophobic core of micelles.[62] As a demonstration, we encapsulated Nile Red in the globular MBB-PP in a phosphate buffer with pH of 9.50. The pH of the solution was then gradually decreased, and fluorescence emission spectra were recorded at selected pH values with an excitation wavelength of 540 nm. Figure 9A shows the fluorescence emission spectra at pH values ranging from 9.50 to 3.50. The maximum fluorescence emission intensity decreased substantially from 400 a.u. at pH = 9.50 to 87 a.u. at pH = 3.50. A two-step release profile of Nile Red can be seen in Figure 9B. The first one occurred in the pH range of 7.5 to 6.5, corresponding to the insoluble-to-soluble transition of PDEAEMA (pK_a = 7.4); the second sharp decrease was observed upon reducing the pH of the solution from ~5.0 to ~4.0, corresponding to the pK_a of PDBAEMA. Note that it is unclear why the fluorescence emission intensity increased with the pH decreasing from 6.0 to 5.0, but this was repeatedly observed in our experiments. The stepwise intensity changes observed here correlated well with the size reduction transitions from DLS measurements (Figure 1A), indicating that the stepwise release of hydrophobic Nile Red from MBB-PP was triggered by the pH-induced conformation changes of MBB-PP. In addition, the maximum peak exhibited a red shift with decreasing pH, from λ_{max} = 578 nm at pH = 9.50 to λ_{max} = 619 nm pH = 3.50, which also indicated that the Nile Red molecules were released from a hydrophobic to a hydrophilic environment. Interestingly, stepwise changes in λ_{max} were also observed, suggesting stepwise polarity changes in the microenvironment of Nile Red with decreasing pH.

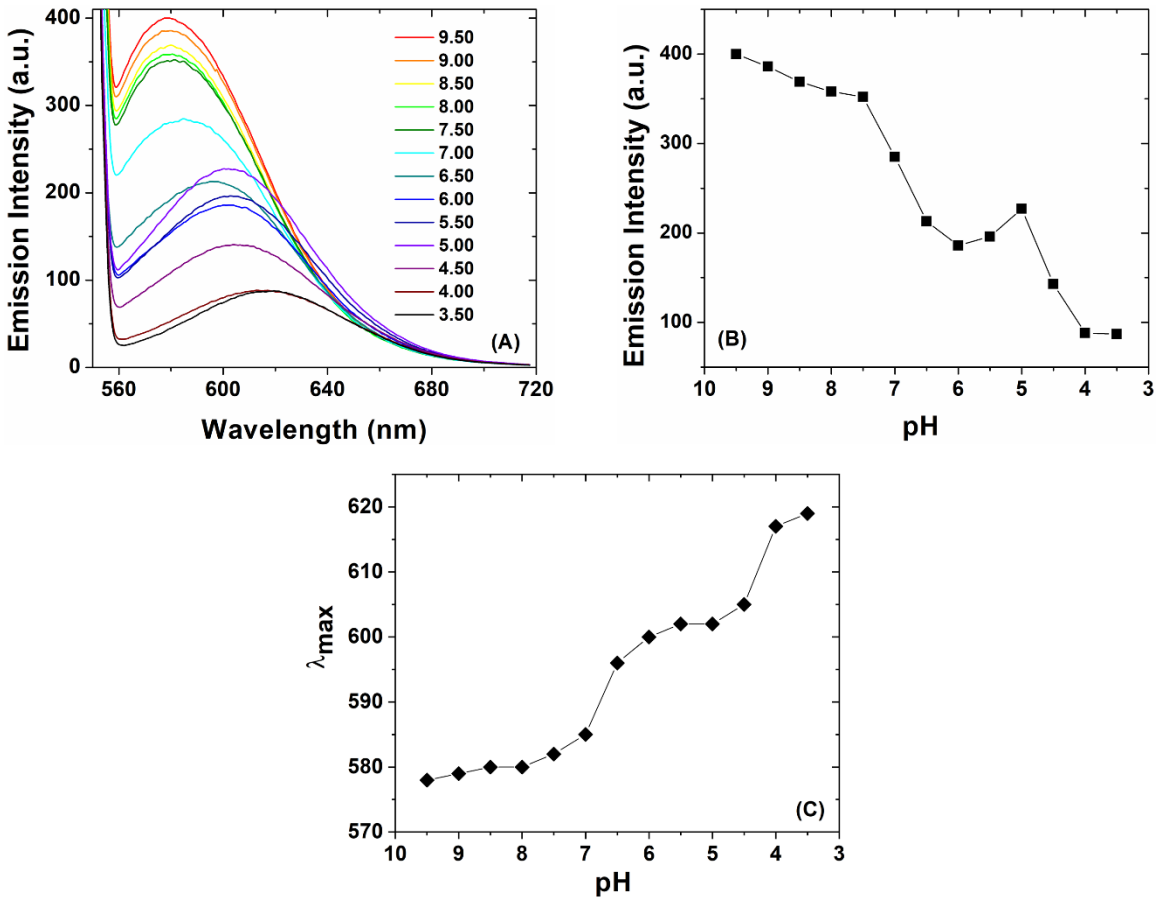

Figure 9. (A) Fluorescence emission spectra of Nile Red in a 4.0 mL solution of 0.2 mg/g MBB-PP in a 25 mM phosphate buffer with decreasing pH from 9.50 to 3.50. The nominal concentration of Nile Red was 6.7×10^{-7} M. The pH of the solution was decreased at a step of 0.50 pH unit, and at each pH the sample was equilibrated for 10 min before the fluorescence emission spectrum was taken. The excitation wavelength is 540 nm, and the spectra were recorded from 550 to 720 nm. (B) Plot of fluorescent emission intensity at the maximum peak versus pH. (C) Plot of λ_{max} versus pH.

Conclusions

Three dually responsive linear ternary heterografted MBBs were synthesized by a grafting to method via the CuAAC click reaction: MBB-PP with two different pH-responsive polymers, MBB-TT with two distinct thermoresponsive polymers, and MBB-TP with one pH-responsive polymer and one thermoresponsive polymer along with 5 kDa PEO as the side chains. DLS studies showed that all three brush polymers exhibited two steplike size reduction transitions in aqueous solution in response to external stimuli, resulting in overall hydrodynamic size decreases by 27%

to 29 % (61% to 64 % decrease in hydrodynamic volume). The size transitions were driven by the pH-induced soluble-to-insoluble and/or temperature-triggered LCST transitions of responsive side chain polymers of the brushes in aqueous solution, which were confirmed by ^{1}H NMR spectroscopy analysis. AFM imaging revealed stepwise conformational changes from extended wormlike brushes (with and without a pearl-necklace morphology) to partially collapsed nanostructures (shrunken wormlike or wavelike or C-/S-shaped) to globular nano-objects stabilized by PEO side chains. This work shows that it is possible to achieve controllable stepwise conformational transitions of multicomponent MBBs while maintaining the stability of brush molecules against aggregation in solution, opening up more opportunities for potential applications in diverse areas such as drug delivery, stimuli-responsive emulsions, and controlled templated synthesis of nanomaterials. As a demonstration, MBB-PP was used to encapsulate Nile Red as a hydrophobic model drug in the globular state, and a stepwise release profile was achieved upon gradually decreasing pH.

ORCID

Bin Zhao: 0000-0001-5505-9390

Supporting Information. Experimental Section, calculation of grafting densities and absolute molecular weights, and additional characterization data. The Supporting Information is available free of charge on the ACS Publications website at DOI: xxxxxxxxxxxxx.

Acknowledgements: This work was supported by NSF through DMR-2004564.

References

1. Zhang, M. F.; Müller, A. H. E. Cylindrical Polymer Brushes. *J. Polym. Sci. Part A: Polym. Chem.* **2005**, *43*, 3461-3481.

2. Sheiko, S. S.; Sumerlin, B. S.; Matyjaszewski, K. Cylindrical Molecular Brushes: Synthesis, Characterization, and Properties. *Prog. Polym. Sci.* **2008**, *33*, 759-785.
3. Lee, H.-I.; Pietrasik, J.; Sheiko, S. S.; Matyjaszewski, K. Stimuli-Responsive Molecular Brushes. *Prog. Polym. Sci.* **2010**, *35*, 24-44.
4. Rzayev, J. Molecular Bottlebrushes: New Opportunities in Nanomaterials Fabrication. *ACS Macro Lett.* **2012**, *1*, 1146-1149.
5. Xie, G.; Martinez, M. R.; Olszewski, M.; Sheiko, S. S.; Matyjaszewski, K. Molecular Bottlebrushes as Novel Materials. *Biomacromolecules* **2019**, *20*, 27-54.
6. Zhao, B. Shape-Changing Bottlebrush Polymers. *J. Phys. Chem. B* **2021**, *125*, 6373-6389.
7. Liao, L.; Liu, J.; Dreaden, E. C.; Morton, S. W.; Shopsowitz, K. E.; Hammond, P. T.; Johnson, J. A. A Convergent Synthetic Platform for Single-Nanoparticle Combination Cancer Therapy: Ratiometric Loading and Controlled Release of Cisplatin, Doxorubicin, and Camptothecin. *J. Am. Chem. Soc.* **2014**, *136*, 5896–5899.
8. Luo, H.; Szymusiak, M.; Garcia, E. A.; Lock, L. L.; Cui, H.; Liu, Y.; Herrera-Alonso, M. Solute-Triggered Morphological Transitions of an Amphiphilic Heterografted Brush Copolymer as a Single-Molecule Drug Carrier. *Macromolecules* **2017**, *50*, 2201-2206.
9. Runge, M. B.; Bowden, N. B. Synthesis of High Molecular Weight Comb Block Copolymers and Their Assembly into Ordered Morphologies in the Solid State. *J. Am. Chem. Soc.* **2007**, *129*, 10551-10560.
10. Xia, Y.; Olsen, B. D.; Kornfield, J. A.; Grubbs, R. H. Efficient Synthesis of Narrowly Dispersed Brush Copolymers and Study of Their Assemblies: The Importance of Side Chain Arrangement. *J. Am. Chem. Soc.* **2009**, *131*, 18525-18532.
11. Liberman-Martin, A. L.; Chu, C. K.; Grubbs, R. H. Application of Bottlebrush Block Copolymers as Photonic Crystals. *Macromol. Rapid Commun.* **2017**, *38*, 1700058.
12. Daniel , W. F.; Burdynska, J.; Vatankhah-Varnoosfaderani, M.; Matyjaszewski, K.; Paturej, J.; Rubinstein, M.; Dobrynin, A. V.; Sheiko, S. S. Solvent-Free, Supersoft and Superelastic Bottlebrush Melts and Networks. *Nat. Mater.* **2016**, 15, 183-189.
13. Sheiko, S. S.; Dobrynin, A. V. Architectural Code for Rubber Elasticity: From Supersoft to Superfirm Materials. *Macromolecules* **2019**, *52*, 7531-7546.
14. Banquy, X.; Burdyńska, J.; Lee, D. W.; Matyjaszewski, K.; Israelachvili, J. Bioinspired Bottle-Brush Polymer Exhibits Low Friction and Amontons-Like Behavior. *J. Am. Chem. Soc.* **2014**, *136*, 6199 -6202.
15. Qi, H.; Liu, X. T.; Henn, D. M.; Mei, S.; Staub, M. C.; Zhao, B.; Li, C. Y. Breaking Translational Symmetry via Polymer Chain Overcrowding in Molecular Bottlebrush Crystallization. *Nature Communications* **2020**, *11*, 2152.
16. Henn, D. M.; Fu, W. X.; Mei, S.; Li, C. Y.; Zhao, B. Temperature-Induced Shape Changing of Thermosensitive Binary Heterografted Linear Molecular Brushes between Extended Worm-Like and Stable Globular Conformations. *Macromolecules* **2017**, *50*, 1645-1656.
17. Sheiko, S. S.; Prokhorova, S. A.; Beers, K. L.; Matyjaszewski, K.; Potemkin, I. I.; Khokhlov, A. R.; Möller, M. Single Molecule Rod−Globule Phase Transition for Brush Molecules at a Flat Interface. *Macromolecules* **2001,** *34,* 8354-8360.
18. Boyce, J. R.; Shirvanyants, D.; Sheiko, S. S.; Ivanov, D. A.; Qin, S. H.; Börner, H.; Matyjaszewski, K. Multiarm Molecular Brushes: Effect of the Number of Arms on the Molecular Weight Polydispersity and Surface Ordering. *Langmuir* **2004**, *20*, 6005-6011.

19. Sun, F.; Sheiko, S. S.; Moeller, M.; Beers, K.; Matyjaszewski, K. Conformational Switching of Molecular Brushes in Response to the Energy of Interaction with the Substrate. *J. Phys. Chem. A* **2004**, *108*, 9682–9686.
20. Gallyamov, M. O.; Tartsch, B.; Khokhlov, A. R.; Sheiko, S. S.; Börner, H. G.; Matyjaszewski, K.; Möller, M. Reversible Collapse of Brushlike Macromolecules in Ethanol and Water Vapours as Revealed by Real-Time Scanning Force Microscopy. *Chem. Eur. J.* **2004,** *10*, 4599-4605.
21. Gallyamov, M. O.; Tartsch, B.; Khoklov, A. R.; Sheiko, S. S.; Börner, H. G.; Matyjaszewski, K.; Möller, M. Real-Time Scanning Force Microscopy of a Macromolecular Conformational Transitions. *Macromol. Rapid Comm.* **2004**, *25*, 1703-1707.
22. Li, C.; Gunari, N.; Fischer, K.; Janshoff, A.; Schmidt, M. New Perspectives for the Design of Molecular Actuators: Thermally Induced Collapse of Single Macromolecules from Cylindrical Brushes to Spheres. *Angew. Chem. Int. Ed.* **2004**, *43*, 1101-1104.
23. Lee, H.-I.; Pietrasik, J.; Matyjaszewski, K. Phototunable Temperature-Responsive Molecular Brushes Prepared by ATRP. *Macromolecules* **2006**, *39*, 3914–3920.
24. Lee, H.-I.; Boyce, J.R.; Nese, A.; Sheiko, S. S.; Matyjaszewski, K. pH-Induced Conformational Changes of Loosely Grafted Molecular Brushes Containing Poly(acrylic acid) Side Chains. *Polymer* **2008**, *49*, 5490-5496.
25. Yamamoto, S.-i.; Pietrasik, J.; Matyjaszewski, K. ATRP Synthesis of Thermally Responsive Molecular Brushes from Oligo(ethylene oxide) Methacrylates. *Macromolecules* **2007**, *40,* 9348-9353.
26. Pietrasik, J.; Sumerlin, B.S.; Lee, R.Y.; Matyjaszewski, K. Solution Behavior of Temperature-Responsive Molecular Brushes Prepared by ATRP. *Macromol. Chem. Phys.* **2007**, *208*, 30–36.
27. Stephan, T.; Muth, S.; Schmidt, M. Shape Changes of Statisical Copolymacromomers: From Wormlike Cylinders to Horseshoe- and Meanderlike Structures. *Macromolecules* **2002**, *35*, 9857-9860.
28. Gunari, N.; Cong, Y.; Zhang, B.; Fischer, K.; Janshoff, A.; Schmidt, M. Surfactant-Induced Helix Formation of Cylindrical Brush Polymers with Poly(L-lysine) Side Chains. *Macromol. Rapid Commun.* **2008**, *29*, 821-825.
29. Xu, Y.; Bolisetty, S.; Drechsler, M.; Fang, B.; Yuan, J.; Harnau, L.; Ballauff, M.; Müller, A. X. E. Manipulating Cylindrical Polyelectrolyte Brushes on the Nanoscale by Counterions: Collapse Transition to Helical Structures. *Soft Matter* **2009**, *5*, 379–384.
30. Xu, Y.; Bolisetty, S.; Ballauff, M.; Müller, A. H. E. Switching the Morphologies of Cylindrical Polycation Brushes by Ionic and Supramolecular Inclusion Complexes. *J. Am. Chem. Soc.* **2009**, *131*, 1640–1641.
31. Xu, Y.; Borisov, O. V.; Ballauff, M.; Muller, A. H. Manipulating the Morphologies of Cylindrical Polyelectrolyte Brushes by Forming Interpolyelectrolyte Complexes with Oppositely Charged Linear Polyelectrolytes: an AFM Study. *Langmuir* **2010,** *26*, 6919-6926.
32. Weller, D.; McDaniel, J. R.; Fischer, K.; Chilkoti, A.; Schmidt, M. Cylindrical Polymer Brushes with Elastin-Like Polypeptide Side Chains. *Macromolecules* **2013**, *46*, 4966-4971.
33. Li, X.; ShamsiJazeyi, H.; Pesek, S. L.; Agrawal, A.; Hammouda, B.; Verduzco, R. Thermoresponsive PNIPAAM Bottlebrush Polymers with Tailored Side-Chain Length and End-Group Structure. *Soft Matter* **2014**, *10*, 2008-2015.

34. Kutnyanszky, E.; Hempenius, M. A.; Vancso, G. J. Polymer Bottlebrushes with a Redox Responsive Backbone Feel the Heat: Synthesis and Characterization of Dual Responsive Poly(ferrocenylsilane)s with PNIPAM Side Chains. *Polym. Chem.* **2014**, *5*, 771-783.
35. Zhu, X. M.; Zhang, J.; Miao, C.; Li, S. Y.; Zhao, Y. L. Synthesis, Thermoresponsivity and Multi-Tunable Hierarchical Self-assembly of Multi-Responsive $(AB)_mC$ Miktobrush-Coil Terpolymers. *Polym. Chem.* **2020**, *11*, 3003-3017.
36. Yan, Y. Y.; Gao, C.; Li, J. J.; Zhang, T.; Yang, G.; Wang, Z. K.; Hua, Z. Modulating Morphologies and Surface Properties of Nanoparticles from Cellulose-Grafted Bottlebrush Copolymers Using Complementary Hydrogen-Bonding between Nucleobases. *Biomacromolecules* **2020**, *21*, 613-620.
37. Henn, D. M.; Lau, C. M.; Li, C. Y.; Zhao, B. Light-Triggered Unfolding of Single Linear Molecular Bottlebrushes from Compact Globular to Wormlike Nano-Objects in Water. *Polym. Chem.* **2017**, *8*, 2702-2712.
38. Henn, D. M.; Holmes, J. A.; Kent, E. W.; Zhao, B. Worm-to-Sphere Shape Transition of Thermoresponsive Linear Molecular Bottlebrushes in Moderately Concentrated Aqueous Solution. *J. Phys. Chem. B* **2018**, *122*, 7015-7025.
39. Kent, E. W.; Henn, D. M.; Zhao, B. Shape-Changing Linear Molecular Bottlebrushes with Dually pH- and Thermo-Responsive Diblock Copolymer Side Chains. *Polym. Chem.* **2018**, *9*, 5133-5144.
40. Kent, E. W.; Zhao, B. Stimuli-Induced Star-Globule Shape Transitions of Dually Responsive Binary Heterografted Three-Arm Star Molecular Brushes in Aqueous Solution. *Macromolecules* **2019**, *52(17)*, 6714-6724.
41. Kent, E. W.; Lewoczko, E. M.; Zhao, B. pH- and Chaotropic Anion-Induced Conformational Changes of Tertiary Amine-Containing Binary Heterografted Star Molecular Bottlebrushes in Aqueous Solution. *Polymer Chemistry* **2021**, *12*, 265-276.
42. Lewoczko, E. M.; Kelly, M. T.; Kent, E. W.; Zhao, B. Effects of Temperature on Chaotropic Anion-Induced Shape Transitions of Star Molecular Bottlebrushes with Heterografted Poly(ethylene oxide) and Poly(N,N-dialkylaminoethyl methacrylate) Side Chains in Acidic Water. *Soft Matter* **2021**, *17*, 6566-6579.
43. Gumus, B.; Herrera-Alonso, M.; Ramírez-Hernández, A. Kinetically-Arrested Single-Polymer Nanostructures from Amphiphilic Mikto-Grafted Bottlebrushes in Solution: a Simulation Study. *Soft Matter* **2020**, *16*, 4969-4979.
44. Gumerov, R. A.; Potemkin, I. I. Computer Simulations of Comb-Like Macromolecules with Responsive Diblock Copolymer Side Chains. *Colloid Polym. Sci.* **2021**, *299*, 407-418.
45. Gao, H. F.; Matyjaszewski, K. Synthesis of Molecular Brushes by "Grafting onto" Method: Combination of ATRP and Click Reactions. *J. Am. Chem. Soc.* **2007**, *129*, 6633– 6639.
46. Tang, H.; Li, Y.; Lahasky, S. H.; Sheiko, S. S.; Zhang, D. Core−Shell Molecular Bottlebrushes with Helical Polypeptide Backbone: Synthesis, Characterization, and Solution Conformations. *Macromolecules* **2011**, *44*, 1491-1499.
47. Han, D.; Tong, X.; Zhao Y. One-Pot Synthesis of Brush Diblock Copolymers through Simultaneous ATRP and Click Coupling. *Macromolecules* **2011**, *44*, 5531-5536.
48. Zhao, P.; Yan, Y.; Feng, X.; Liu, L.; Wang, C.; Chen, Y. Highly Efficient Synthesis of Polymer Brushes with PEO and PCL as Side Chains via Click Chemistry. *Polymer* **2012**, *53*, 1992-2000.
49. Li, Y.; Themistou, E.; Zou, J.; Das, B. P.; Tsianou, M.; Cheng, C. Facile Synthesis and Visualization of Janus Double-Brush Copolymers. *ACS Macro Lett.* **2012**, *1*, 52–56.

50. Kent, E. W.; Lewoczko, E. M.; Zhao, B. Effect of Buffer Anions on Pearl-Necklace Morphology of Tertiary Amine-Containing Binary Heterografted Linear Molecular Bottlebrushes in Acidic Aqueous Buffers. *Langmuir* **2020**, *36*, 13320-13330.
51. Jin, N. X.; Woodcock, J. W., Xue, C. M.; O'Lenick, T. G.; Jiang, X. G.; Jin, S.; Dadmun, M. D.; Zhao, B. Tuning of Thermo-Triggered Gel-to-Sol Transition of Aqueous Solution of Multi-Responsive Diblock Copolymer Poly(methoxytri(ethylene glycol) acrylate-*co*-acrylic acid)-*b*-poly(ethoxydi(ethylene glycol) acrylate). *Macromolecules* **2011**, *44*, 3556-3566.
52. Woodcock, J. W., Jiang, X. G.; Wright, R. A. E.; Zhao, B. Enzyme-Induced Formation of Thermoreversible Micellar Gels from Aqueous Solutions of Multiresponsive Hydrophilic ABA Triblock Copolymers. *Macromolecules* **2011**, *44*, 5764-5775.
53. Hua, F. J.; Jiang, X. G.; Li, D. J.; Zhao, B. Well-Defined Thermosensitive, Water-Soluble Polyacrylates and Polystyrenics with Short Pendant Oligo(ethylene glycol) Groups Synthesized by Nitroxide-Mediated Radical Polymerization. *J. Polym. Sci. Part A: Polym. Chem.* **2006**, *44*, 2454-2467.
54. Zhou, K. J.; Wang, Y. G.; Huang, X. N.; Luby-Phelps, K.; Sumer, B. D.; Gao, J. M. Tunable, Ultrasensitive pH-Responsive Nanoparticles Targeting Specific Endocytic Organelles in Living Cells. *Angew. Chem., Int. Ed.* **2011**, *50*, 6109 -6114
55. Henn, D. M.; Wright, R. A. E.; Woodcock, J. W.; Hu, B.; Zhao, B. Tertiary Amine-Containing Thermo- and pH-Sensitive Hydrophilic ABA Triblock Copolymers: Effect of Different Tertiary Amines on Thermally Induced Sol-Gel Transitions. *Langmuir* **2014**, *30*, 2541–2550.
56. Chiefari, J.; Chong, Y. K.; Ercole, F.; Krstina, J.; Jeffery, J.; Le, T. P. T.; Mayadunne, R. T. A.; Meijs, G. F.; Moad, C. L.; Moad, G.; Rizzardo, E.; Thang, S. H. Living Free-Radical Polymerization by Reversible Addition-Fragmentation Chain Transfer: The RAFT Process. *Macromolecules* **1998**, *31*, 5559-5562.
57. Zhang, M.; Drechsler, M.; Müller, A. H. E. Template-Controlled Synthesis of Wire-Like Cadmium Sulfide Nanoparticle Assemblies within Core−Shell Cylindrical Polymer Brushes. *Chem. Mater.* **2004**, *16*, 537–543.
58. Zhang, M.; Estournès, C.; Bietsch, W.; Müller, A. H. E. Superparamagnetic Hybrid Nanocylinders. *Adv. Funct. Mater.* **2004**, *14*, 871–882.
59. Schild, H. G. Poly(*N*-isopropylacrylamide): Experiment, Theory and Application. *Prog. Polym. Sci.* **1992**, *17*, 163-249.
60. Lewoczko, E. M.; Wang, N.; Lundberg, C. E.; Kelly, M. T.; Kent, E. W.; Wu, T.; Chen, M.-L.; Wang, J.-H.; Zhao, B. Effects of *N*-Substituents on Solution Behavior of Poly(sulfobetaine methacrylate)s in Water: UCST and LCST. *ACS Applied Polymer Materials* **2021**, *3*, 867-878.
61. Potemkin, I. I.; Khokhlov, A. R.; Prokhorova, S.; Sheiko, S. S.; Möller, M.; Beers, K. L.; Matyjaszewski, K. Spontaneous Curvature of Comblike Polymers at a Flat Interface. *Macromolecules* **2004**, *37*, 3918-3923.
62. Jiang, X. G.; Lavender, C. A.; Woodcock, J. W.; Zhao, B. Multiple Micellization and Dissociation Transitions of Thermo- and Light-Sensitive Poly(ethylene oxide)-*b*-poly(ethoxytri(ethylene glycol) acrylate-*co*–*o*-nitrobenzyl acrylate) in Water. *Macromolecules* **2008**, *41*, 2632-2643.